

MANTONIELLA BEAUFORTII AND *MANTONIELLA BAFFINENSIS* SP.

NOV. (MAMIELLALES, MAMIELLOPHYCEAE),

TWO NEW GREEN ALGAL SPECIES FROM THE HIGH ARCTIC¹

Sheree Yau²

Integrative Marine Biology Laboratory (BIOM), CNRS, UMR7232, Sorbonne Université,

Banyuls sur Mer, France.

Adriana Lopes dos Santos

Sorbonne Université, CNRS, UMR7144, Station Biologique de Roscoff, Roscoff, France.

Centro de Genómica, Ecología y Medio Ambiente, Facultad de Ciencias, Universidad Mayor.

Camino La Pirámide 5750, Huechuraba. Santiago, Chile.

Asian School of the Environment, Nanyang Technological University, 50 Nanyang Avenue,

Singapore

Wenche Eikrem

Norwegian Institute for Water Research, Gaustadall  n 21, 0349, Oslo, Norway.

University of Oslo, Department of Biosciences, P.O. box 1066 Blindern, 0316, Oslo, Norway.

Natural History Museum, University of Oslo, P.O. box 1172 Blindern, 0318 Oslo, Norway.

Catherine Gérikas Ribero and Priscilla Gourvil

Sorbonne Université, CNRS, UMR7144, Station Biologique de Roscoff, Roscoff, France.

Sergio Balzano

Stazione Zoologica Anton Dohrn, Istituto Nazionale di Biologia, Ecologia e Biotecnologie

Marine, Naples, Italy.

23 Marie-Line Escande and Hervé Moreau
24 Integrative Marine Biology Laboratory (BIOM), CNRS, UMR7232, Sorbonne Université,
25 Banyuls sur Mer, France.
26 Daniel Vaultot
27 Sorbonne Université, CNRS, UMR7144, Station Biologique de Roscoff, Roscoff, France.
28 Asian School of the Environment, Nanyang Technological University, 50 Nanyang Avenue,
29 Singapore.
30
31 Corresponding author: Sheree Yau, sheeyau@gmail.com
32 Running Title: *Mantoniella* species from the high Arctic
33

34 *Abstract*

35 Members of the class Mamiellophyceae comprise species that can dominate
36 picophytoplankton diversity in polar waters. Yet polar species are often morphologically
37 indistinguishable from temperate species, although clearly separated by molecular features. Here
38 we examine four Mamiellophyceae strains from the Canadian Arctic. The 18S rRNA and
39 Internal Transcribed Spacer 2 (ITS2) gene phylogeny place these strains within the family
40 Mamiellaceae (Mamiellales, Mamiellophyceae) in two separate clades of the genus *Mantoniella*.
41 ITS2 synapomorphies support their placement as two new species, *Mantoniella beaufortii* and
42 *Mantoniella baffinensis*. Both species have round green cells with diameter between 3–5 µm, one
43 long flagellum and a short reduced flagellum (~1 µm) and are covered by spiderweb-like scales,
44 making both species similar to other *Mantoniella* species. Morphologically, *M. beaufortii* and
45 *M. baffinensis* are most similar to the cosmopolitan *M. squamata* with only minor differences in
46 scale structure distinguishing them. Screening of global marine metabarcoding datasets indicates
47 *M. beaufortii* has only been recorded in seawater and sea ice samples from the Arctic while no
48 environmental barcode matches *M. baffinensis*. Like other Mamiellophyceae genera that have
49 distinct polar and temperate species, the polar distribution of these new species suggests they are
50 cold or ice-adapted *Mantoniella* species.

51 Keywords: *Mantoniella*, Mamiellophyceae, polar, Arctic, picophytoplankton, ITS,
52 metabarcoding

53 Abbreviations: rRNA, ribosomal RNA; ITS2, internal transcribed spacer 2; compensatory
54 base change, CBC; hemi-CBC, hCBC; TEM, transmission electron microscopy.

56 *Introduction*

57 Over the last decades the taxonomy of the green algae has gone through a profound
58 reorganization. The class Prasinophyceae, initially defined as scaly flagellates (Throndsen and
59 Moestrup 1988), has been rearranged into many new classes such as the Chlorodendrophyceae,
60 Chloropicophyceae and Mamiellophyceae (Massjuk 2006, Marin and Melkonian 2010, Lopes
61 dos Santos et al. 2017b) leading to the name Prasinophyceae to be abandoned. The
62 Mamiellophyceae are ecologically successful and particularly dominant in marine coastal waters
63 (Lopes dos Santos et al. 2017a, Tragin and Vaulot 2018). The first scaled species of
64 Mamiellophyceae observed were *Mantoniella squamata* (Manton et Parke) Desikachary
65 (originally *Micromonas squamata*), in 1960 (Manton and Parke 1960), and *Mamiella gilva*
66 (Parke et Rayns) Moestrup (originally *Nephroselmis gilva*), in 1964 (Moestrup 1984). Moestrup
67 (1984) erected the family Mamiellaceae, which included *Mantoniella* and *Mamiella*, with
68 *Mamiella gilva* designated as the type species. The class Mamiellophyceae comprises three
69 orders: the Monomastigales, with one freshwater genus *Monomastix*; Dolichomastigales, with
70 two genera *Crustomastix* and *Dolichomastix*; and the Mamiellales, which currently comprises
71 five genera *Bathycoccus*, *Mamiella*, *Mantoniella*, *Micromonas* and *Ostreococcus*. As these
72 genera are morphologically heterogeneous, with *Micromonas* and *Ostreococcus* lacking scales
73 and *Bathycoccus* and *Ostreococcus* lacking flagella, the monophyly of Mamiellophyceae was
74 established based on nuclear and plastid rRNA sequence and secondary structure analyses
75 (Marin and Melkonian 2010).

76 Molecular analyses of the Mamiellophyceae have permitted the description of otherwise
77 morphologically indistinguishable cryptic species. For example, wide genetic diversity has been
78 shown to exist between morphologically identical *Ostreococcus* species where less than 1%

79 difference in the 18S rRNA gene corresponds to up to 30% of variation in orthologous protein
80 coding sequences (Palenik et al. 2007, Piganeau et al. 2011). From an early stage, 18S rRNA
81 defined clades of *Micromonas* and *Ostreococcus* were observed to correspond to distinct
82 geographic distributions, suggesting their genetic variation reflects adaptations to ecological
83 niches (Rodríguez et al. 2005, Foulon et al. 2008), and that these clades represent distinct
84 species. *Ostreococcus* is divided into rare species restricted to estuarine (*O. mediterraneus*) and
85 coastal environments (*O. tauri*), as well as more abundant oceanic species (*O. lucimarinus* and
86 clade B) (Demir-Hilton et al. 2011, Treusch et al. 2012, Hu et al. 2016, Simmons et al. 2016). In
87 *Micromonas*, the species *M. polaris* appears to be specially adapted to polar environments, while
88 the other species are restricted to lower latitudes (Not et al. 2005, Lovejoy et al. 2007, Balzano et
89 al. 2012b, Simon et al. 2017). Similarly, in *Mantoniella*, *M. antarctica* was described from the
90 Antarctic while *M. squamata* is cosmopolitan (Marchant et al. 1989).

91 Three picophytoplanktonic strains (RCC2285, RCC2288 and RCC2497) were isolated in the
92 Canadian Arctic from mesophilic surface water sampled at two sites in the Beaufort Sea in the
93 summer of 2009 as part of the MALINA cruise (Balzano et al. 2012a). A fourth strain was
94 subsequently isolated from sea ice collected in Baffin Bay in the spring as part of the Green Edge
95 project. We performed a combination of molecular, morphological and pigment characterization
96 of these isolates, which we propose to constitute two novel *Mantoniella* species, *M. beaufortii*
97 and *M. baffinensis*, restricted to polar environments.

98 *Methods*

99 *Culture conditions*

100 Strains RCC2285, RCC2288, and RCC2497 were isolated from seawater collected at two
101 sites ($70^{\circ}30'N$, $135^{\circ}30'W$ and $70^{\circ}34'N$, $145^{\circ}24'W$) in the Beaufort Sea in the summer of 2009 as
102 part of the MALINA cruise as described previously (Balzano et al. 2012a). Strain RCC5418 was
103 isolated from the Green Edge project Ice Camp (<http://www.greenedgeproject.info/>), a sampling
104 site on the sea ice near the village of Qikiqtarjuaq ($67^{\circ}28.784'N$, $63^{\circ}47.372'W$). Sampling was
105 conducted between 20 April and 27 July, 2016, beginning in completely snow covered
106 conditions followed by bare ice and ending when the ice was broken out. Sea ice from 23 May
107 2016 was melted overnight and 200 ml was gravity filtered (Sartorius filtration system) through
108 3 μm pore size polycarbonate filters (Millipore Isopore membrane, 47 mm). 500 μL of filtrate
109 was enriched by addition to 15 ml of L1 medium (NCMA, Bigelow Laboratory for Ocean
110 Sciences, USA). The enrichment culture was purified by dilution to 10 cells per well in a 96
111 deep-well plate (Eppendorf) and incubated under white light ($100 \mu E m^{-2} s^{-1}$) in a 12:12 h light:
112 dark cycle at $4^{\circ}C$. Cell growth was observed by the development of coloration after a few weeks.
113 Culture purity was assessed by flow cytometry (Becton Dickinson, Accuri C6). After
114 confirmation of the purity, the culture was transferred in a 50 ml ventilated flask (Sarstedt).
115 Cultures are maintained in the Roscoff Culture Collection (<http://roscoff-culture-collection.org/>)
116 in K/2 (Keller et al. 1987) or L1 medium at $4^{\circ}C$ under a 12:12 h light: dark cycle at $100 \mu E$ light
117 intensity. RCC2285 has been lost from culture since molecular analyses (described below) were
118 performed. For pigment analysis and electron microscopy, RCC2288 was grown at $7^{\circ}C$ under
119 continuous light at $100 \mu E$ intensity in L1 medium prepared using autoclaved seawater from

120 offshore Mediterranean Sea water diluted 10% with MilliQ water and filtered prior to use
121 through 0.22 µm filters.

122 *Sequences*

123 Nuclear 18S rRNA and the Internal Transcribed Spacers (ITS) 1 and 2, as well as the 5.8S
124 rRNA gene were retrieved from GenBank for strains RCC2288, RCC2497 and RCC2285
125 (Balzano et al. 2012a). For RCC5418 and RCC5150 (*M. antarctica*), cells were harvested in
126 exponential growth phase and concentrated by centrifugation. Total nucleic acids were extracted
127 using the Nucleospin Plant II kit (Macherey-Nagel, Düren, DE) following the manufacturer's
128 instructions. The nearly full length nuclear 18S rRNA gene (only RCC5418) and the region
129 containing the Internal Transcribed Spacers (ITS) 1 and 2, as well as the 5.8S rRNA gene were
130 obtained by PCR amplification using universal primers (Supplementary Table 1).

131 PCR products were directly sequenced at the Macrogen Company (Korea) and sequences
132 have been deposited to Genbank under accession numbers MH516003, MH516002 and
133 MH542162.

134 *Phylogenetic analyses*

135 Nuclear 18S rRNA sequences belonging to members of Mamiellophyceae were retrieved
136 from GenBank (<http://www.ncbi.nlm.nih.gov/>). Two environmental sequences (similar to strain
137 sequences) were included in addition to the sequences obtained from the cultures. Sequences
138 were also obtained for the ITS2 region located between the 5S and 23S rRNA genes. However,
139 no environmental sequences were available to be included in the 18S/ITS phylogenetic analyses.

140 Nuclear 18S rRNA and ITS2 sequences were aligned with MAFFT using the E-INS-i and G-
141 INS-i algorithms respectively (Katoh and Toh 2008). For each sequence within the ITS2
142 alignment, the preliminary secondary structure annotated in dot-bracket format was associated,
143 generating a Vienna file, which was imported to 4SALE (Seibel et al. 2008). The final alignment
144 was edited on the basis of conserved secondary structures. The nuclear 18S rRNA and ITS2
145 sequences from the Mamiellaceae members were concatenated using Geneious 10.2.5 (Kearse et
146 al. 2012).

147 Phylogenetic reconstructions with two different methods, maximum likelihood (ML) and
148 Bayesian analyses, were performed using the nuclear Mamiellophyceae 18S rRNA and
149 Mamiellaceae concatenated 18S/ITS2 alignments. The K2 + G + I model was selected for both
150 sequence datasets based on the substitution model selected through the Akaike information
151 criterion (AIC) and the Bayesian information criterion (BIC) options implemented in MEGA
152 6.06 (Tamura et al. 2013). ML analysis was performed using PhyML 3.0 (Guindon et al. 2010)
153 with SPR (Subtree Pruning and Regrafting) tree topology search operations and approximate
154 likelihood ratio test with Shimodaira-Hasegawa-like procedure. Markov chain Monte Carlo
155 iterations were conducted for 1,000,000 generations sampling every 100 generations with
156 burning length 100,000 using MrBayes 3.2.2 (Ronquist and Huelsenbeck 2003) as implemented
157 in Geneious (Kearse et al. 2012). Nodes were considered as well supported when SH-like
158 support values and Bayesian posterior probabilities were higher than 0.8 and 0.95 respectively.
159 The same criteria were used to represent the sequences on the phylogenetic trees. Alignments are
160 available at <https://doi.org/10.6084/m9.figshare.7472153.v1>.

161 *ITS2 secondary structure*

162 ITS2 secondary structure from the strains listed in Table 1 were predicted using the Mfold
163 web interface (Zuker 2003) under the default options with the folding temperature fixed at 37°C,
164 resulting in multiple alternative folding patterns per sequence. The preliminary structure for each
165 sequence was chosen based on similarities found among the other structures proposed for
166 Mamiellophyceae (Marin and Melkonian 2010, Simon et al. 2017) as well as on the presence of
167 previously defined ITS2 hallmarks defined by Coleman (Mai and Coleman 1997, Coleman 2000,
168 2003, 2007). Exported secondary structures in Vienna format and the respective nucleotide
169 sequences were aligned, visualized using 4SALE version 1.7 (Seibel et al. 2008) and manually
170 edited through extensive comparative analysis of each position (nucleotide) in sequences from
171 representatives of the Mamiellophyceae. The ITS2 synapomorphy analysis was confined to
172 those positions, which formed conserved base pairs in all members of the Mamiellaceae order
173 and the resulting intramolecular folding pattern (secondary structure) of *Mantoniella* was drawn
174 using CorelDRAW X7. A Vienna file containing the ITS2 sequences and secondary structure is
175 available at <https://doi.org/10.6084/m9.figshare.7472153.v1>.

176 *Screening of environmental 18S rRNA sequencing datasets*

177 High-throughput sequencing metabarcodes (V4 and V9 hypervariable regions) were obtained
178 from several published polar studies, as well as from the global sampling efforts Tara Oceans
179 and Ocean Sampling Day (OSD) (see Supplementary Table 2 for the full details and references
180 for each project). We screened these data as well as GenBank by BLASTn (98% identity cut-off)
181 using RCC2288 18S rRNA gene sequence as the search query. We aligned the retrieved
182 environmental sequences and metabarcodes with that of RCC2285, RCC2288, RCC2497, and

183 RCC5418 using MAFFT as implemented in Geneious version 10.0.7 (Kearse et al. 2012). This
184 allowed the determination of sequence signatures diagnostic of this species for both V4 and V9
185 (Supplementary Figures 1 and 2). The oceanic distribution of stations where cultures, clones and
186 metabarcodes having these signatures, as well as the stations from the metabarcoding surveys
187 where no matching metabarcodes have been found, were plotted with the R libraries ggplot2 and
188 rworldmap. The R script is available at <https://vaulot.github.io/papers/RCC2288.html>.

189 *Light microscopy*

190 Cells were observed using an Olympus BX51 microscope (Olympus, Hamburg, Germany)
191 with a 100 \times objective using differential interference contrast (DIC) and imaged with a SPOT
192 RT-slider digital camera (Diagnostics Instruments, Sterling Heights, MI, USA).

193 For video-microscopy, cultures from RCC2288 and RCC2497 were observed with an inverted
194 Olympus IX70 inverted microscope using an x40 objective and equipped with an Infinity X
195 camera (<https://www.lumenera.com/products/microscopy/infinityx-32.html>). Short sequences
196 were recorded and edited with the Video de Luxe software (<http://www.magix.com/fr/video-deluxe/>). Films were uploaded to Youtube (<https://www.youtube.com/channel/UCsYoz-aSJIJesyDNj6ZVolQ/videos>). The recording protocol is available at
197 <https://www.protocols.io/private/1fbc54800109d5f44e88574f40194ed1>

200 *Transmission Electron Microscopy*

201 Positively stained whole mount cells were prepared described (Moestrup 1984) where cultures
202 were directly deposited on formvar coated copper grids and stained with 2% uranyl acetate. TEM
203 thin-sections was performed as previously described (Derelle et al. 2008). Briefly, fixed

204 RCC2288 cells (1% glutaraldehyde) from an exponentially growing culture were suspended in
205 molten (37°C) 1% low melting point agarose. The agarose cell plug was fixed, washed,
206 dehydrated in ethanol and embedded in Epon 812. Ultra-thin sections (80–90 nm) were placed
207 on a 300 mesh copper grid and stained with uranyl acetate for 15 min, followed by lead citrate
208 staining for 2 min. The cells were visualised with Hitachi H 7500 and H-9500 transmission
209 electron microscopes.

210 *Pigment analysis*

211 Pigments were extracted from RCC2288 cells in late exponential phase as previously
212 described (Ras et al. 2008). Briefly, cells were collected on 0.7 µm particle retention size filters
213 (GF/F Whatman), pigments extracted for 2 hours in 100% methanol, then subjected to ultrasonic
214 disruption and clarified by filtration through 0.2 µm pore-size filters (PTFE). Pigments were
215 detected using high performance liquid chromatography (HPLC, Agilent Technologies 1200)
216 over the 24 h after the extraction.

217 *Results and Discussion*

218 *Taxonomy section*

219 *Mantoniella beaufortii* Yau, Lopes dos Santos and Eikrem sp. nov.
220 Diagnosis: Cells round measuring 3.7 ± 0.4 µm in diameter with one long (16.3 ± 2.6 µm) and
221 one short reduced flagellum (~1 µm). Cell body and flagella covered in imbricated spiderweb
222 scales. Flagellar hair scales present composed of two parallel rows of subunits. Long flagellum
223 tip has tuft of three hair scales. Scales produced in Golgi body. Golgi body located beneath and

224 to the side of basal bodies. One green chloroplast with pyrenoid surrounded by starch and a
225 stigma composed of a single layer of oil droplets (ca 0.1 μm). Ejectosomes composed of fibrils
226 located at periphery of cell. Cell bodies with sub-quadrangular to oval scales (~0.2 μm). Body
227 scales heptaradial, with seven major spokes radiating from center, number of spokes increasing
228 in number towards the periphery. Six or more concentric ribs divide the scale into segments.
229 Flagella with hexaradial oval scales composed of six spokes increasing in number towards the
230 periphery. Six or more concentric ribs divide the scale into segments. Combined nucleotide
231 sequences of the 18S rRNA (JN934679) and rRNA ITS2 (JQ413369) are species specific. In
232 ITS2 of the nuclear encoded rRNA operon, base pair 4 of Helix I is C-G instead of U-A and base
233 pair 22 of Helix IV is G-C instead of G-U.

234 Holotype: Plastic embedding deposited at the Natural History Museum, University of Oslo,
235 accession numbers O-A-10010. Figure 4 shows cells from the embedding. Culture deposited in
236 The Roscoff Culture Collection as RCC2288.

237 Type locality: Strain RCC2288 was isolated from surface water sampled from the Beaufort
238 Sea in the Arctic Ocean ($70^{\circ}30'\text{N}$, $135^{\circ}30'\text{W}$) on 14th July 2009.

239 Etymology: Named for its geographical provenance.

240

241 *Mantoniella baffinensis* Yau, Lopes dos Santos and Eikrem sp. nov.

242 Diagnosis: Cells measuring $4.7 \pm 0.5 \mu\text{m}$ with a long flagellum of $21.8 \pm 5.1 \mu\text{m}$ and one
243 short reduced flagellum (~1 μm). Cell body and flagella covered in imbricated spiderweb scales.
244 Flagellar hair scales present composed of two parallel rows of subunits. Long flagellum tip has
245 tuft of three hair scales. Cell bodies with sub-quadrangular to oval scales (~0.2 μm). Body scales
246 octaradial with eight major radial spokes radiating from center, number of spokes increasing in

247 number towards the periphery. Seven or more concentric ribs divide the scale into segments.
248 Flagella with heptaradial, oval scales composed of seven spokes increasing in number towards
249 the periphery. Six or more concentric ribs divide the scale into segments. Combined nucleotide
250 sequences of the nuclear 18S rRNA (MH516003) and rRNA ITS2 (MH542162) are species
251 specific. In ITS2 of the nuclear encoded rRNA operon, base pair 9 of Helix I is C-G instead of
252 A-U, base pair 15 of Helix II is G-C instead of A-U and base pair 22 of Helix IV is C-G instead
253 of G-U.

254 Holotype: Plastic embedding deposited at the Natural History Museum, University of Oslo,
255 accession number O-A-10011. Culture deposited in The Roscoff Culture Collection as
256 RCC5418.

257 Type locality: Strain RCC5418 was isolated from surface sea ice sampled off the coast of
258 Baffin Island, in the Baffin Bay (67°28'N, 63°46'W) on 23th May 2016.

259 Etymology: Named for its geographical provenance.

260 *Phylogeny and ITS signatures*

261 The phylogenetic tree based on nearly full-length nuclear 18S rRNA sequences obtained from
262 the novel polar strains RCC2288, RCC2285, RCC2497 and RCC5418 (Table 1), and
263 environmental sequences retrieved from GenBank indicate that these strains belong to the family
264 Mamiellaceae (Supplementary Figure 3). The analysis also recovers the major genera within the
265 order Mamiellales: *Bathycoccus*, *Ostreococcus*, *Micromonas*, *Mantoniella* and *Mamiella* (Marin
266 and Melkonian 2010). Dolichomastigales and Monomastigales were the basal orders in the class
267 Mamiellophyceae with the *Monomastix opisthostigma* type species used as an outgroup. The
268 three strains isolated during the MALINA cruise in the Beaufort Sea (RCC2485, RCC2288 and

269 RCC2497) and the strain from the Baffin Bay (RCC5418) form a well-supported clade together
270 with two environmental sequences (clone MALINA St320 3m Nano ES069 D8 and clone 4-E5),
271 also originated from Arctic Ocean samples. The two described *Mantoniella* species
272 (*M. squamata* and *M. antarctica*) are not monophyletic in our analysis using the nuclear 18S
273 rRNA, as observed by Marin and Melkonian (2010) (Supplementary Figure 3).

274 In contrast, the phylogenetic tree based on concatenated 18S/ITS2 alignments suggests that
275 our strains belong to the genus *Mantoniella* (Figure 1). The topology of the concatenated
276 18S/ITS tree, in addition to grouping our strains within *Mantionella*, is consistent with a recent
277 nuclear multigene phylogeny based on 127 concatenated genes from related Chlorophyta species
278 that included RCC2288 (Lopes dos Santos et al. 2017b). This indicates the 18S/ITS2 tree reflects
279 the evolutionary history of the nuclear genome supporting the position of *Mantoniella* and our
280 strains diverging from the same common ancestor.

281 The average distance between strains RCC2485, RCC2288 and RCC2497 is low (0.5% of
282 segregating sites over the near full-length 18S rRNA gene), suggesting that these strains
283 correspond to a single species that we name *Mantoniella beaufortii* (see taxonomy section). In
284 contrast, the well-supported placement of strain RCC5418 on an earlier diverging branch within
285 the *Mantoniella* clade, as well as the 1% average distance between RCC5418 and the other
286 strains, suggests it represents another species, named here *Mantoniella baffinensis*.

287 To substantiate the description of *M. beaufortii* and *M. baffinensis* as new species, we
288 investigated ITS2 synapomorphies of the different *Mantoniella* species. Several studies have
289 shown the power of using ITS2 sequences in delimiting biological species, especially in
290 microalgae studies (e.g. Coleman 2007, Caisová et al. 2011, Lopes dos Santos et al. 2017b,
291 Simon et al. 2017). For example, ITS sequencing contributed to distinguishing the Arctic diatom

292 *Chaetoceros neogracilis* from an Antarctic *Chaetoceros* sp. that share nearly identical 18S rRNA
293 genes (Balzano et al. 2017). Moreover, nucleotide diversity within the ITS2 allowed the
294 identification of four distinct populations within the Beaufort Sea. The computed ITS2 secondary
295 structure of the new *Mantoniella* strains contains the four helix domains found in many
296 eukaryotic taxa (Supplementary Figure 4), in addition to the presence of Helix B9. The
297 intramolecular folding pattern of the ITS2 transcript from *M. beaufortii* and *M. baffinensis* is
298 very similar to the one from *M. squamata* and *M. antarctica* (Supplementary Figure 4). The
299 universal hallmarks proposed by Mai and Coleman et al. (1997) and Schultz et al. (2005) are
300 present in Helices II and III of the Mamiellaceae. These are the Y-Y (pyrimidine-pyrimidine)
301 mismatch at conserved base pair 7 in Helix II (Figure 2) and YRRY (pyrimidine-purine-
302 pyrimidine) motif at conserved positions 28–31 on the 5' side of Helix III (Supplementary Figure
303 5A). In all four strains, the Y-Y mismatch is represented by the pair U-U and the YRRY motif by
304 the sequence UGGU.

305 The structural comparison at each base pair position within the ITS2 helices identified
306 several compensatory base changes (CBCs) and single-side changes or hemi-CBCs (hCBCs), as
307 well as conserved base pair positions among *Mantoniella* species (Supplementary Figure 4).
308 Note that we only considered hCBCs at positions where the nucleotide bond was preserved. No
309 CBCs was found between the three *M. beaufortii* strains consistent with their designation as a
310 single species. However, three hCBCs were detected in Helix II at positions 15 and 17 (Figure 2)
311 and Helix III at position 12 (Supplementary Figure 5A). Three CBCs were detected in Helices I
312 (position 4), II (position 15) and IV (position 22) between *M. beaufortii* and *M. baffinensis*,
313 supporting the separation of these strains into two distinct species (Figure 2 and Supplementary
314 Figure 4). When possible, the evolutionary steps of the identified CBCs and hCBCs were

315 mapped upon branches of the Mamiellaceae phylogenetic tree that was constructed based on the
316 concatenated 18S/ITS2 (Figure 2 and Supplementary Figure 4) to distinguish synapomorphies
317 from homoplasious changes (e.g. parallelisms and reversals). Few hypervariable positions
318 showing several changes (CBCs and hCBCs) could not be unambiguously mapped upon the tree.

319 *Morphology and ultrastructure*

320 Under light microscopy, the cells of the new strains are green and round with one long and
321 one short reduced flagellum (~1 µm), which are inserted almost perpendicularly to the cell
322 (Figure 3). They swim with their flagella directed posteriorly, pushing the cell. Occasionally the
323 cells cease movement, pirouette and take off again in a different direction (Supplementary
324 Material 1–3). All strains possess a stigma, visible in light microscopy as a red eyespot located
325 opposite the flagella. Although there are no morphological characters that are unique to the
326 mamiellophyceans and shared by all of its members, the new strains closely resemble
327 *Mantoniella* and *Mamiella*, which are similarly small round bi-flagellated cells (see
328 Supplementary Table 3 for morphological characters in described Mamiellophyceae). However,
329 the flagella of *Mamiella* are of equal or near equal lengths (Moestrup 1984), so clearly the
330 unequal flagella observed in our strains conform with described *Mantoniella* species,
331 *M. squamata* and *M. antarctica* (Barlow and Cattolico 1980, Marchant et al. 1989). The new
332 strains are thus morphologically indistinguishable by light microscopy from *Mantoniella* species,
333 supporting their placement in the genus.

334 The new strains are in the size range (Table 2) reported for *M. squamata* (3–6.5 µm) and
335 *M. antarctica* (2.8–5 µm) (Manton and Parke 1960, Marchant et al. 1989). Nonetheless,
336 *M. beaufortii* strains are significantly smaller than *M. baffinensis* in cell diameter and average

337 long flagellum length (Table 2) providing a means to distinguish the two new *Mantoniella*
338 species from each other with light microscopy.

339 Transmission Electron Microscopy (TEM) of thin sections (Figure 4) and whole mounts
340 (Figure 5) of the new strains provided details of their internal and external morphological
341 features. The single chloroplast is green and cup-shaped with a pyrenoid surrounded by starch
342 tubules running through the pyrenoid. The stigma is composed of a single layer of oil droplets
343 (approximately 0.1 µm in diameter) (Figure 4A) and located at the periphery of the chloroplast
344 facing the cell membrane, conforming to the description of the family Mamiellaceae (Marin and
345 Melkonian 2010). Several large ejectosomes composed of fibrils are present at the cell periphery
346 (Figure 4D and E). They are common in the Mamiellales (Moestrup 1984, Marchant et al. 1989)
347 and are perhaps used to deter grazers.

348 One of the most salient features of the Mamiellophyceae is the presence of organic scales
349 covering the cell, the most common of which comprise radiating and concentric ribs resembling
350 spiderwebs that are present in the scale-bearing Mamiellales (*Bathycoccus*, *Mamiella* and
351 *Mantoniella*), as well as *Dolichomastix* (Supplementary Table 3). We examined the whole
352 mounts of the new *Mantoniella* species to establish the presence of scales and determine if they
353 were morphologically distinguishable from related species, as *M. antarctica* (Marchant et al.
354 1989) and *M. gilva* (Moestrup 1984) each have a unique type that differentiate them from other
355 Mamiellales.

356 The flagella and cell bodies of the new strains are covered in imbricated spiderweb-like scales
357 (Figure 5) measuring approximately 0.2 µm. The scales are produced in the Golgi body (Figure
358 4B). The body scales are sub-quadrangular to oval whereas the flagellar scales are oval (Figure
359 5). Spiderweb scales have 6–8 major spokes radiating from the center with the number of spokes

360 increasing in number towards the periphery and six or more concentric ribs dividing the scale
361 into segments. In addition, there are some small scales (approximately 0.1 µm) on the cell body
362 composed of four spokes (increasing to eight) and separated by four, more or less concentric,
363 ribs (Figure 5D, G). The flagella are also covered by lateral hair scales, which are composed of
364 two parallel rows of globular subunits. At the tip of the long flagellum there is a tuft of three hair
365 scales, for which the subunits are more closely packed together than the lateral hair scales
366 (Figure 5). The hair scales of the new strains are identical to the "Tetraselmis-type" T-hairs
367 previously described in *Mantoniella* and *Mamiella* (Marin and Melkonian 1994). This structure
368 is otherwise only seen in *Dolichomastix lepidota* and differs from the smooth tubular T-hairs of
369 *Dolichomastix tenuilepis* and *Crustomastix* (Marin and Melkonian 1994, Zingone et al.
370 2002)(Supplementary Table 3).

371 Comparison of the spiderweb scales between *Mantoniella* species (Table 3) shows the new
372 species differ significantly from *M. antarctica*, which possesses lace-like scales with six or seven
373 radial ribs with very few concentric ribs (Marchant et al. 1989). Morphologically, the spiderweb
374 scales of the new species most resemble *M. squamata*, which has large heptaradial flagellar
375 scales, octaradial body scales and a few additional small tetraradial body scales (Marchant et al.
376 1989). Indeed, the spiderweb scales of *M. baffinensis* (Figure 5) are structurally indistinguishable
377 from *M. squamata*. In contrast, *M. beaufortii* shares the small tetraradial body scales but
378 possesses hexaradial flagellar scales and heptaradial body scales, potentially allowing it to be
379 differentiated from the other *Mantoniella* based on the number of radial spokes of the spiderweb
380 scales.

381 *Pigment composition*

382 Pigment to chlorophyll *a* ratios of *M. beaufortii* RCC2288 were compared to a selection of
383 other Chlorophyta species (Figure 6, Supplementary Table 4) from previous studies (Latasa et al.
384 2004, Lopes dos Santos et al. 2016), as pigments are useful phenotypic traits. Chlorophyll *a* and
385 *b*, characteristics of Chlorophyta, were detected, as well as the basic set of carotenoids found in
386 the prasinophytes: neoxanthin, violaxanthin, lutein, zeaxanthin, antheraxanthin and β-carotene.
387 The additional presence of prasinoxanthin, micromonal and uriolide places RCC2288 in the
388 PRASINO-3B group of prasinophyte green algae, *sensu* Jeffrey et al. (2011). This pigment-based
389 grouping shows good agreement with the molecular phylogeny of Mamiellales, where the
390 presence of prasinoxanthin, micromonal and the Unidentified M1 pigment are diagnostic of the
391 order (Marin and Melkonian 2010). We did not detect Unidentified M1 in RCC2288, but as our
392 analysis method differed from previous work (Latasa et al. 2004) and we relied on matching its
393 chromatographic and spectral characteristics, its absence requires further confirmation.
394 Notwithstanding, the pigment complement of RCC2288 is identical to other described
395 Mamiellales (Figure 6, Supplementary Table 4), coherent with its classification within this order.

396 As noted by Latasa et al. (2004), Mamiellales pigment profiles are remarkably comparable
397 (Figure 6), despite strains being cultured under very different conditions. Only a few carotenoids
398 differed substantially (at least two fold) in relative abundance between *M. beaufortii* and the two
399 other *M. squamata* strains analyzed: the concentration of neoxanthin, antheraxanthin and lutein
400 were higher, whereas that of Mg-DVP and uriolide were relatively lower (Figure 6,
401 Supplementary Table 4). Neoxanthin (associated with the light harvesting complex), as well as
402 antheraxanthin and lutein (both involved in photoprotection), have previously been shown to
403 increase significantly in *M. squamata* grown under continuous light compared to alternating

404 light/dark cycles (Böhme et al. 2002). Therefore, the relatively high ratio of these carotenoids
405 measured in *M. beaufortii* is consistent with growth under continuous light used with RCC2288.
406 Uriolide and Mg-DVP have been observed to increase with light intensity in *M. squamata*
407 (Böhme et al. 2002) and *Micromonas pusilla* (Laviale and Neveux 2011), respectively. Although
408 more physiological data are required to interpret their relative decrease in RCC2288, these
409 pigments are probably most responsive to light conditions (intensity and photoperiod).

410 Two unknown carotenoids were detected in RC2288, the first one having adsorption peaks at
411 412, 436 and 464 nm, and the second one at 452 nm (Supplementary Table 5). These were
412 relatively minor components comprising 2.7% and 1.5% of total carotenoids, respectively and
413 may represent carotenoids unique to *M. beaufortii*.

414 *Environmental distribution*

415 In order to obtain information on the distribution of these two new species, we searched by
416 BLAST both environmental GenBank sequences and published 18S V4 and V9 metabarcodes
417 data sets (Supplementary Table 2). This allowed the retrieval of a few 18S rRNA sequences with
418 higher than 98% similarity to the gene of RCC2288. Alignment of these sequences with other
419 Mamiellophyceae sequences revealed diagnostic positions in both the V4 and V9 hypervariable
420 regions permitting *M. beaufortii* and *M. baffinensis* to be distinguished from other
421 Mamiellophyceae, especially other *Mamiella* and *Mantoniella* species (Supplementary Figures 1
422 and 2). Signatures from the V4 region were clearer than from V9 due to the fact that for some of
423 the strains, the sequences did not extend to the end of the V9 region (Supplementary Figure 2).
424 In the V4 region, three signatures were observed, one common to both species (A in

425 Supplementary Figure 1), while the other two (B and C in Supplementary Figure 1) differed
426 between *M. beaufortii* and *baffinensis*.

427 No clone library or metabarcode sequences matched exactly *M. baffinensis*. In contrast, three
428 environmental sequences (KT814860, FN690725, JF698785) from clone libraries had signatures
429 similar to the *M. beaufortii* strains, two from Arctic Ocean water (Figure 7), including one
430 obtained during the MALINA cruise, and one from ice originating from the Gulf of Finland. V4
431 metabarcodes corresponding to *M. beaufortii* were found in the Ocean Sampling Day data set
432 (Kopf et al. 2015) that includes more than 150 coastal samples at a single station off East
433 Greenland as well as in three metabarcoding studies in the Arctic Ocean, one in the Beaufort Sea
434 performed during the MALINA cruise (Monier et al. 2015), one from Arctic sea ice (Stecher et
435 al. 2016) where it was found at three stations and one from the White Sea (Belevich et al. 2017),
436 also in the sea ice (Figure 7). No metabarcode corresponding to these two new species were
437 found in waters from either the Southern Ocean or off Antarctica (Figure 7 and Supplementary
438 Table 2). No metabarcodes from the V9 region corresponding to the two new species were
439 found in the Tara Oceans data set that covered mostly temperate and subtropical oceanic regions
440 (de Vargas et al. 2015). These data suggest that these species are restricted to polar Arctic
441 regions (although we cannot exclude that they may be found in the future in the Antarctic which
442 has been under-sampled until now) and are probably associated to sea ice although they can be
443 present in the sea water, and that *M. beaufortii* is more wide spread than *M. baffinensis*.

444 *Funding*

445 Financial support for this work was provided by the following projects: ANR PhytoPol (ANR-
446 15-CE02-0007) and Green Edge (ANR-14-CE01-0017-03), ArcPhyt (Région Bretagne),
447 TaxMArc (Research Council of Norway, 268286/E40).

448 *Acknowledgments*

449 We are thankful to Adam Monier, Katja Metfies, Estelle Kilias and Wei Luo for communicating
450 raw metabarcoding data and Sophie Le Panse and Antje Hofgaard for assistance with electron
451 microscopy. We thankful for the support of the BioPIC flow cytometry and microscopy
452 platform of the Oceanological Observatory of Banyuls and of the ABIMS bioinformatics
453 platform at the Roscoff Biological Station.

454

455 *References*

- 456 Balzano, S., Gourvil, P., Siano, R., Chanoine, M., Marie, D., Lessard, S., Sarno, D. et al. 2012a.
457 Diversity of cultured photosynthetic flagellates in the North East Pacific and Arctic Oceans
458 in summer. *Biogeosciences*. 9:4553–71.
- 459 Balzano, S., Marie, D., Gourvil, P. & Vaultot, D. 2012b. Composition of the summer
460 photosynthetic pico and nanoplankton communities in the Beaufort Sea assessed by T-
461 RFLP and sequences of the 18S rRNA gene from flow cytometry sorted samples. *ISME J.*
462 6:1480–98.
- 463 Balzano, S., Percopo, I., Siano, R., Gourvil, P., Chanoine, M., Marie, D., Vaultot, D. et al. 2017.
464 Morphological and genetic diversity of Beaufort Sea diatoms with high contributions from
465 the *Chaetoceros neogracilis* species complex. *J. Phycol.* 53:161–87.
- 466 Barlow, S.B. & Cattolico, R.A. 1980. Fine structure of the scale-covered green flagellate
467 *Mantoniella squamata* (Manton et Parke) Desikachary. *Br. Phycol. J.* 15:321–33.
- 468 Belevich, T.A., Ilyash, L. V., Milyutina, I.A., Logacheva, M.D., Goryunov, D. V. & Troitsky, A.
469 V. 2017. Photosynthetic Picoplankton in the Land-Fast Ice of the White Sea, Russia.
470 *Microb. Ecol.* 1–16.
- 471 Böhme, K., Wilhelm, C. & Goss, R. 2002. Light regulation of carotenoid biosynthesis in the
472 prasinophycean alga *Mantoniella squamata*. *Photochem. Photobiol. Sci.* 1:619–28.
- 473 Caisová, L., Marin, B. & Melkonian, M. 2011. A close-up view on ITS2 evolution and
474 speciation - a case study in the Ulvophyceae (Chlorophyta, Viridiplantae). *BMC Evol. Biol.*
475 11:262.
- 476 Coleman, A.W. 2000. The significance of a coincidence between evolutionary landmarks found
477 in mating affinity and a DNA sequence. *Protist.* 151:1–9.

- 478 Coleman, A.W. 2003. ITS2 is a double-edged tool for eukaryote evolutionary comparisons.
- 479 *Trends Genet.* 19:370–5.
- 480 Coleman, A.W. 2007. Pan-eukaryote ITS2 homologies revealed by RNA secondary structure.
- 481 *Nucleic Acids Res.* 35:3322–9.
- 482 de Vargas, C., Audic, S., Henry, N., Decelle, J., Mahe, F., Logares, R., Lara, E. et al. 2015.
- 483 Eukaryotic plankton diversity in the sunlit ocean. *Science.* 348:1261605.
- 484 Demir-Hilton, E., Sudek, S., Cuvelier, M.L., Gentemann, C.L., Zehr, J.P. & Worden, A.Z. 2011.
- 485 Global distribution patterns of distinct clades of the photosynthetic picoeukaryote
- 486 *Ostreococcus*. *ISME J.* 5:1095–107.
- 487 Derelle, E., Ferraz, C., Escande, M.L., Eychenié, S., Cooke, R., Piganeau, G., Desdevises, Y. et
- 488 al. 2008. Life-cycle and genome of Otv5, a Large DNA virus of the pelagic marine
- 489 unicellular green alga *Ostreococcus tauri*. *PLoS One.* 3.
- 490 Foulon, E., Not, F., Jalabert, F., Cariou, T., Massana, R. & Simon, N. 2008. Ecological niche
- 491 partitioning in the picoplanktonic green alga *Micromonas pusilla*: Evidence from
- 492 environmental surveys using phylogenetic probes. *Environ. Microbiol.* 10:2433–43.
- 493 Guindon, S., Dufayard, J.-F., Lefort, V. & Anisimova, M. 2010. New algorithms and methods to
- 494 estimate maximum-likelihood phylogenies: Assessing the performance of PhyML 3.0.
- 495 *Syst. Biol.* 59:307–21.
- 496 Hu, Y.O.O., Karlson, B., Charvet, S. & Andersson, A.F. 2016. Diversity of pico- to
- 497 mesoplankton along the 2000 km salinity gradient of the baltic sea. *Front. Microbiol.* 7:1–
- 498 17.
- 499 Jeffrey, S.W., Wright, S.W. & Zapata, M. 2011. Microalgal classes and their signature pigments.
- 500 Cambridge Univ Press, Cambridge. 3-77 pp.

- 501 Katoh, K. & Toh, H. 2008. Recent developments in the MAFFT multiple sequence alignment
502 program. *Brief. Bioinform.* 9:286–98.
- 503 Kearse, M., Moir, R., Wilson, A., Stones-Havas, S., Cheung, M., Sturrock, S., Buxton, S. et al.
504 2012. Geneious Basic: An integrated and extendable desktop software platform for the
505 organization and analysis of sequence data. *Bioinformatics*. 28:1647–9.
- 506 Keller, M.D., Selvin, R.C., Claus, W. & Guillard, R.R.L. 1987. Media for the culture of oceanic
507 ultraphytoplankton. *J. Phycol.* 23:633–8.
- 508 Kopf, A., Bicak, M., Kottmann, R., Schnetzer, J., Kostadinov, I., Lehmann, K., Fernandez-
509 Guerra, A. et al. 2015. The ocean sampling day consortium. *Gigascience*. 4:27.
- 510 Latasa, M., Scharek, R., Le Gall, F. & Guillou, L. 2004. Pigment suites and taxonomic groups in
511 Prasinophyceae. *J. Phycol.* 40:1149–55.
- 512 Laviale, M. & Neveux, J. 2011. Relationships between pigment ratios and growth irradiance in
513 11 marine phytoplankton species. *Mar. Ecol. Prog. Ser.* 425:63–77.
- 514 Lopes dos Santos, A., Gourvil, P., Rodríguez, F., Garrido, J.L. & Vaulot, D. 2016.
515 Photosynthetic pigments of oceanic Chlorophyta belonging to Prasinophytes clade VII. *J.*
516 *Phycol.* 52:148–55.
- 517 Lopes dos Santos, A., Gourvil, P., Tragin, M., Noël, M.H., Decelle, J., Romac, S. & Vaulot, D.
518 2017a. Diversity and oceanic distribution of prasinophytes clade VII, the dominant group of
519 green algae in oceanic waters. *ISME J.* 11:512–28.
- 520 Lopes dos Santos, A., Pollina, T., Gourvil, P., Corre, E., Marie, D., Garrido, J.L., Rodríguez, F.
521 et al. 2017b. Chloropicophyceae, a new class of picophytoplanktonic prasinophytes. *Sci.*
522 *Rep.* 7:14019.
- 523 Lovejoy, C., Vincent, W.F., Bonilla, S., Roy, S., Martineau, M.J., Terrado, R., Potvin, M. et al.

- 524 2007. Distribution, phylogeny, and growth of cold-adapted picoprasinophytes in arctic seas.
- 525 *J. Phycol.* 43:78–89.
- 526 Mai, J.C. & Coleman, A.W. 1997. The internal transcribed spacer 2 exhibits a common
- 527 secondary structure in green algae and flowering plants. *J. Mol. Evol.* 44:258–71.
- 528 Manton, I. & Parke, M. 1960. Further observations on small green flagellates with special
- 529 reference to possible relatives of *Chromulina pusilla* Butcher. *J. Mar. Biol. Assoc.* 39:275–
- 530 98.
- 531 Marchant, H.J., Buck, K.R., Garrison, D.L. & Thomsen, H.A. 1989. *Mantoniella* in Antarctic
- 532 waters including the description of *M. antarctica* sp. nov. (Prasinophyceae). *J. Phycol.*
- 533 25:167–74.
- 534 Marin, B. & Melkonian, M. 1994. Flagellar Hairs in Prasinophytes (Chlorophyta): Ultrastructure
- 535 and Distribution on the Flagellar Surface.
- 536 Marin, B. & Melkonian, M. 2010. Molecular phylogeny and classification of the
- 537 Mamiellophyceae class. nov. (Chlorophyta) based on sequence comparisons of the nuclear-
- 538 and plastid-encoded rRNA operons. *Protist.* 161:304–36.
- 539 Massjuk, N.P. 2006. Chlorodendrophyceae class. nov. (Chlorophyta, Viridiplantae) in the
- 540 Ukrainian flora: I. Phylogenetic relations and taxonomical status. *Ukr. Bot. J.* 63:601–14.
- 541 Moestrup, Ø. 1984. Further studies on *Nephroselmis* and its allies (Prasinophyceae). II. *Mamiella*
- 542 gen. nov., Mamiellaceae fam. nov., Mamiellales ord. nov. *Nord. J. Bot.* 4:109–21.
- 543 Monier, A., Me Comte, J., Babin, M., Forest, A., Matsuoka, A. & Lovejoy, C. 2015.
- 544 Oceanographic structure drives the assembly processes of microbial eukaryotic
- 545 communities. *ISME J.* 9:990–1002.
- 546 Not, F., Massana, R., Latasa, M., Marie, D., Colson, C., Eikrem, W., Pedrós-Alió, C. et al. 2005.

- 547 Late summer community composition and abundance of photosynthetic picoeukaryotes in
548 Norwegian and Barents Seas. *Limnol. Oceanogr.* 50:1677–1686.
- 549 Palenik, B., Grimwood, J., Aerts, A., Rouzé, P., Salamov, A., Putnam, N., Dupont, C. et al. 2007.
550 The tiny eukaryote *Ostreococcus* provides genomic insights into the paradox of plankton
551 speciation. *Proc. Natl. Acad. Sci. U. S. A.* 104:7705–10.
- 552 Piganeau, G., Eyre-Walker, A., Grimsley, N. & Moreau, H. 2011. How and why DNA barcodes
553 underestimate the diversity of microbial eukaryotes. *PLoS One.* 6.
- 554 Ras, J., Claustre, H. & Uitz, J. 2008. Spatial variability of phytoplankton pigment distributions in
555 the Subtropical South Pacific Ocean: comparison between *in situ* and predicted data.
556 *Biogeosciences.* 5:353–69.
- 557 Rodríguez, F., Derelle, E., Guillou, L., Le Gall, F., Vaulot, D. & Moreau, H. 2005. Ecotype
558 diversity in the marine picoeukaryote *Ostreococcus* (Chlorophyta, Prasinophyceae).
559 *Environ. Microbiol.* 7:853–9.
- 560 Ronquist, F. & Huelsenbeck, J.P. 2003. MrBAYES 3: Bayesian phylogenetic inference under
561 mixed models. *Bioinformatics.* 19:1572–4.
- 562 Schultz, J., Maisel, S., Gerlach, D., Müller, T. & Wolf, M. 2005. A common core of secondary
563 structure of the internal transcribed spacer 2 (ITS2) throughout the Eukaryota. *RNA.*
564 11:361–4.
- 565 Seibel, P., Müller, T., Dandekar, T. & Wolf, M. 2008. Synchronous visual analysis and editing of
566 RNA sequence and secondary structure alignments using 4SALE. *BMC Res. Notes.* 1:91.
- 567 Simmons, M.P., Sudek, S., Monier, A., Limardo, A.J., Jimenez, V., Perle, C.R., Elrod, V.A. et al.
568 2016. Abundance and biogeography of picoprasinophyte ecotypes and other phytoplankton
569 in the eastern North Pacific Ocean. *Appl. Environ. Microbiol.* 82:1693–705.

- 570 Simon, N., Foulon, E., Grulois, D., Six, C., Desdevises, Y., Latimier, M., Le Gall, F. et al. 2017.
571 Revision of the Genus *Micromonas* Manton et Parke (Chlorophyta, Mamiellophyceae), of
572 the Type Species *M. pusilla* (Butcher) Manton et Parke of the Species *M. commoda* van
573 Baren, Bathy and Worden and Description of Two New Species Based on the Genetic and
574 Phenotypic Characterization of Cultured Isolates. *Protist.* 168:612–35.
- 575 Stecher, A., Neuhaus, S., Lange, B., Frickenhaus, S., Beszteri, B., Kroth, P.G. & Valentin, K.
576 2016. rRNA and rDNA based assessment of sea ice protist biodiversity from the central
577 Arctic Ocean. *Eur. J. Phycol.* 51:31–46.
- 578 Tamura, K., Stecher, G., Peterson, D., Filipski, A. & Kumar, S. 2013. MEGA6: Molecular
579 evolutionary genetics analysis version 6.0. *Mol. Biol. Evol.* 30:2725–9.
- 580 Thronsen, J. & Moestrup, Ø. 1988. Light and electron microscopical studies on
581 *Pseudoscourfieldia marina*, a primitive scaly green flagellate (Prasinophyceae) with
582 posterior flagella. *Can. J. Bot.* 66:1415–34.
- 583 Tragin, M. & Vaulot, D. 2018. Green microalgae in marine coastal waters: The Ocean Sampling
584 Day (OSD) dataset. *Sci. Rep.* 8:1–12.
- 585 Treusch, A.H., Demir-Hilton, E., Vergin, K.L., Worden, A.Z., Carlson, C. a, Donatz, M.G.,
586 Burton, R.M. et al. 2012. Phytoplankton distribution patterns in the northwestern Sargasso
587 Sea revealed by small subunit rRNA genes from plastids. *ISME J.* 6:481–92.
- 588 Zingone, A., Borra, M., Brunet, C., Forlani, G., Kooistra, W.H.C.F. & Procaccini, G. 2002.
589 Phylogenetic position of *Crustomastix stigmatica* sp. nov. and *Dolichomastix tenuilepsis* in
590 relation to the Mamiellales (Prasinophyceae, Chlorophyta). *J. Phycol.* 38:1024–39.
- 591 Zuker, M. 2003. Mfold web server for nucleic acid folding and hybridization prediction. *Nucleic
592 Acids Res.* 31:3406–15.

593 *Figures*

594 Figure 1. Maximum-likelihood tree inferred from concatenated 18S/ITS2 sequences of
595 Mamiellaceae. Solid dots correspond to nodes with significant support (> 0.8) for ML analysis
596 and Bayesian analysis (> 0.95). Empty dots correspond to nodes with non-significant support for
597 either ML or Bayesian analysis, or both.

598

599 Figure 2. Molecular signatures of *Mantoniella* species based on comparison of ITS2
600 secondary structures within Mamiellaceae. Signatures in Helix I are shown in blue and Helix II
601 in red. The conserved base pairs among the different groups are numbered. Compensatory base
602 changes (CBCs) and hemi-CBCs (hCBSs) are highlighted by solid and dotted arrows
603 respectively. Hypervariable positions are marked by an asterisk (*). Ellipsis (...) represent the
604 other clades and species of *Micromonas*. The pyrimidine-pyrimidine (Y-Y) mismatch in Helix II
605 is shown in bold black. Single nucleotide substitutions are shown by grey nucleotides. Identified
606 homoplasious changes are shown as parallelisms and reversals.

607

608 Figure 3. Light microscopy images of the new *Mantoniella* strains. All strains have round cell
609 morphology, visible red stigma (black arrow), a long and short flagellum (white arrow) and one
610 chloroplast with a pyrenoid (white arrowhead). Scale bar is 4 μm for all images. (A–B)
611 *M. beaufortii* RCC2288. (C–D) *M. beaufortii* RCC2497 during cell division and single cell
612 showing long and short flagellum. (E–G) *M. baffinensis* RCC5418 single cell (E), during cell
613 division (F) and cell showing the short flagellum (G inset).

614

615 Figure 4. TEM thin sections of *M. beaufortii* RCC2288. **(A)** Internal cell structure showing
616 organelles and stigma (black arrow). **(B)** Detail of the hair and spiderweb scales covering the
617 long flagellum. Scales are produced in the Golgi body. **(C)** Detail of the flagellar base (black
618 arrow). **(D)** Cell with long and short flagella and longitudinal section of the ejectosomes (black
619 arrow). **(E)** Cross section of ejectosomes (black arrow). **(F)** and **(G)** Body scales made up of
620 radiating and concentric ribs. Abbreviations: e=ejectosome, g=Golgi, s=starch granule,
621 m=mitochondrion, n=nucleus, p=pyrenoid, hs=hair scale, sc=scale, lf=long flagellum and
622 sf=short flagellum.

623

624 Figure 5. Transmission electron micrographs of whole-mounts of the new *Mantoniella* strains.
625 **(A–E)** *M. beaufortii*. **(A)** Whole cells of strain RCC2288, indicating the short flagellum (white
626 arrow), and **(B)** RCC2497. **(C)** Detached flagellar spiderweb-like scales and hair scales (black
627 arrowhead). **(D)** Detail of small tetraradial body scale. **(E)** Imbricated scales and hair scales
628 covering the long flagellum. A tuft of three hair scales on the tip of the long flagellum (black
629 arrow) **(F)** Detail of the tuft of hair scales (black arrow). **(G–H)** *M. baffinensis* RCC5418. **(G)**
630 Small and large body scales (black arrows) and flagellar hair scales (black arrowhead) and **(H)**
631 whole cell.

632

633 Figure 6. Pigment to chlorophyll *a* ratios in *M. beaufortii* RCC2288 (this study) compared to
634 other Mamiellophyceae species (data from Latasa et al. 2004). **(A)** Cumulative pigment to
635 Chlorophyll *a* ratio of Chlorophyll *b* and abundant carotenoids (excluding α - and β -carotene).
636 **(B)** As for A, but showing relative abundances. Mg-DVP: Mg-24-divinyl pheophopyrin *a5*
637 monmethyl ester.

638

639 Figure 7. Map of the distribution of *M. beaufortii* in environmental sequence datasets
640 highlighting its prevalence in Arctic samples (inset). The isolation sites of *M. beaufortii* cultures,
641 presence of its 18S rRNA gene sequence in clone libraries (Clone water, Clone ice) and
642 metabarcodes from seawater and ice samples (Meta water, Meta ice) and absence in
643 metabarcodes (Not found) are plotted. For *M. baffinensis*, only its isolation site is indicated in
644 Baffin Bay since no similar environmental sequence was found in the datasets analyzed.
645 Metabarcoding datasets include Ocean Sampling Day, Tara Oceans and polar projects. See
646 Supplementary Table 2 for a full description of the metabarcoding datasets screened.

647 *Tables*

648 Table 1. Strains used in this study. RCC: Roscoff Culture Collection (www.roscoff-culture-collection.org). 18S rRNA and ITS show Genbank accession numbers. Strains in bold used to
649 describe the new species.

Strain ID	Strain name	Oceanic Region	Latitude	Longitude	Depth of isolation (m)	18S rRNA	ITS	Remark
RCC2285	MALINA E43.N1	Beaufort Sea	70° 34' N	145° 24' W	0	JF794053	JQ413368	Strain lost
RCC2288	MALINA E47.P2	Beaufort Sea	70° 30' N	135° 30' W	0	JN934679	JQ413369	
RCC2497	MALINA E47.P1 GE_IP_IC_DIL	Beaufort Sea	70° 30' N	135° 30' W	0	KT860921	JQ413370	
RCC5418	490	Baffin Bay	67° 28' N	63° 46' W	surface ice	MH51600	MH54216	

651

652 Table 2. Cell diameter and long flagellum lengths measured for *M. beaufortii* (RCC2288 and
653 RCC2497) and *M. baffinensis* (RCC5418). n = number of cells measured and SD = standard
654 deviation.

Strain	min	max	mean	median	stdev	n
Cell diameter (μm)						
RCC2288	2.89	4.98	3.77	3.70	0.41	60
RCC2497	3.15	4.74	3.87	3.77	0.39	39
RCC5418	3.54	5.69	4.66	4.66	0.51	69
Long flagellum length (μm)						
RCC2288	12.93	21.47	16.27	15.99	2.63	11
RCC2497	11.91	21.25	16.31	17.07	2.71	12
RCC5418	11.27	32.59	21.78	21.29	5.14	25

655

656 Table 3. Comparison of *Mantoniella* spp. scale types.

Species	Flagellar scales	Body scales
<i>Mantoniella squamata</i>	spiderweb-like heptaradial	spiderweb-like large octaradial and small rare tetraradial
<i>Mantoniella antarctica</i>	lace-like heptaradial	lace-like hexaradial and smaller heptaradial
<i>Mantoniella beaufortii</i>	spiderweb-like hexaradial	spiderweb-like large heptaradial and small rare tetraradial
<i>Mantoniella baffinensis</i>	spiderweb-like heptaradial	spiderweb-like large octaradial and small rare tetraradial

657

658 *Supplementary Figures*

659 Supplementary Figure 1. Alignment of the 18S rRNA gene V4 hypervariable region from
660 *M. beaufortii* and *M. baffinensis* strains (Red and Orange, respectively), environmental clones
661 (Blue) and metabarcodes (Green) with a selection of sequences from closely related
662 Mamiellophyceae. Sequence signatures diagnostic of the two new species are indicated by boxes.
663 The A region is specific of both species while the B and C regions differ between the two
664 species.

665

666 Supplementary Figure 2. Alignment of the 18S rRNA gene V9 hypervariable region from
667 *M. beaufortii* and *M. baffinensis* strains (Red and Orange, respectively) and environmental
668 clones (blue) with a selection of closely related Mamiellophyceae sequences. Sequence
669 signatures diagnostic of *M. beaufortii* and *M. baffinensis* are indicated by arrows.

670

671 Supplementary Figure 3. Maximum-likelihood phylogenetic tree inferred from nuclear 18S
672 rRNA sequences of Mamiellophyceae. *Monomastix opisthostigma* was used as an outgroup.
673 Solid dots correspond to nodes with significant support (> 0.8) for ML analysis and Bayesian
674 analysis (>0.95). Empty dots correspond to nodes with non-significant support for either ML or
675 Bayesian analysis, or both. GenBank accessions of the 18S rRNA sequences shown after the
676 species name.

677

678 Supplementary Figure 4. Intramolecular folding pattern of the ITS2 molecule of *Mantoniella*
679 (RCC2288, RCC2285, RCC2497 and RCC5418). The four major helices are labeled as Helix I –
680 Helix IV. Blue dots represent either CBCs or hCBCs. Non-CBCs ($N - N \leftrightarrow N \times N$) are
681 represented in orange.

682

683 Supplementary Figure 5. Molecular signatures of *Mantoniella* species revealed by comparison
684 of ITS2 secondary structures within Mamiellaceae. Signatures in of Helix III are shown in (A)
685 and Helix IV in (B). The conserved base pairs among the different groups are numbered. CBCs
686 and hCBCs are highlighted by solid and dotted arrows, respectively. Hypervariable positions are
687 marked by an asterisk (*). Ellipsis (...) represent the other clades and species of *Micromonas*.
688 The YRRY (pyrimidine-purine-pyrimidine) motif on the 5' side arm of Helix III is shown in

689 bold black. Single nucleotide substitutions are shown by grey nucleotides. Identified
690 homoplasious changes are shown as parallelisms and reversals.

691

692 *Supplementary Tables*

693 Supplementary Table 1. Primers and PCR conditions used in this study. Abbreviations: fwd –
694 forward, rev. – reverse, Temp. – Temperature.

695

696 Supplementary Table 2. Metabarcoding datasets of the 18S rRNA gene analysed in this study
697 for the presence of *M. beaufortii* and *M. baffinensis* signatures.

698

699 Supplementary Table 3. Morphological characters in Mamiellophyceae species.

700

701 Supplementary Table 4. Pigment composition of *M. beaufortii* (RCC2288) compared to a
702 selection of green algae. Values are shown as a ratio of pigment to Chl *a* concentration and
703 percent contribution to total carotenoids (in italics). See Supplementary Table 5 for the full
704 names of the pigments.

705

706 Supplementary Table 5. Pigments analyzed in this study. LOD, limit of detection.

707

708 *Supplementary Material*

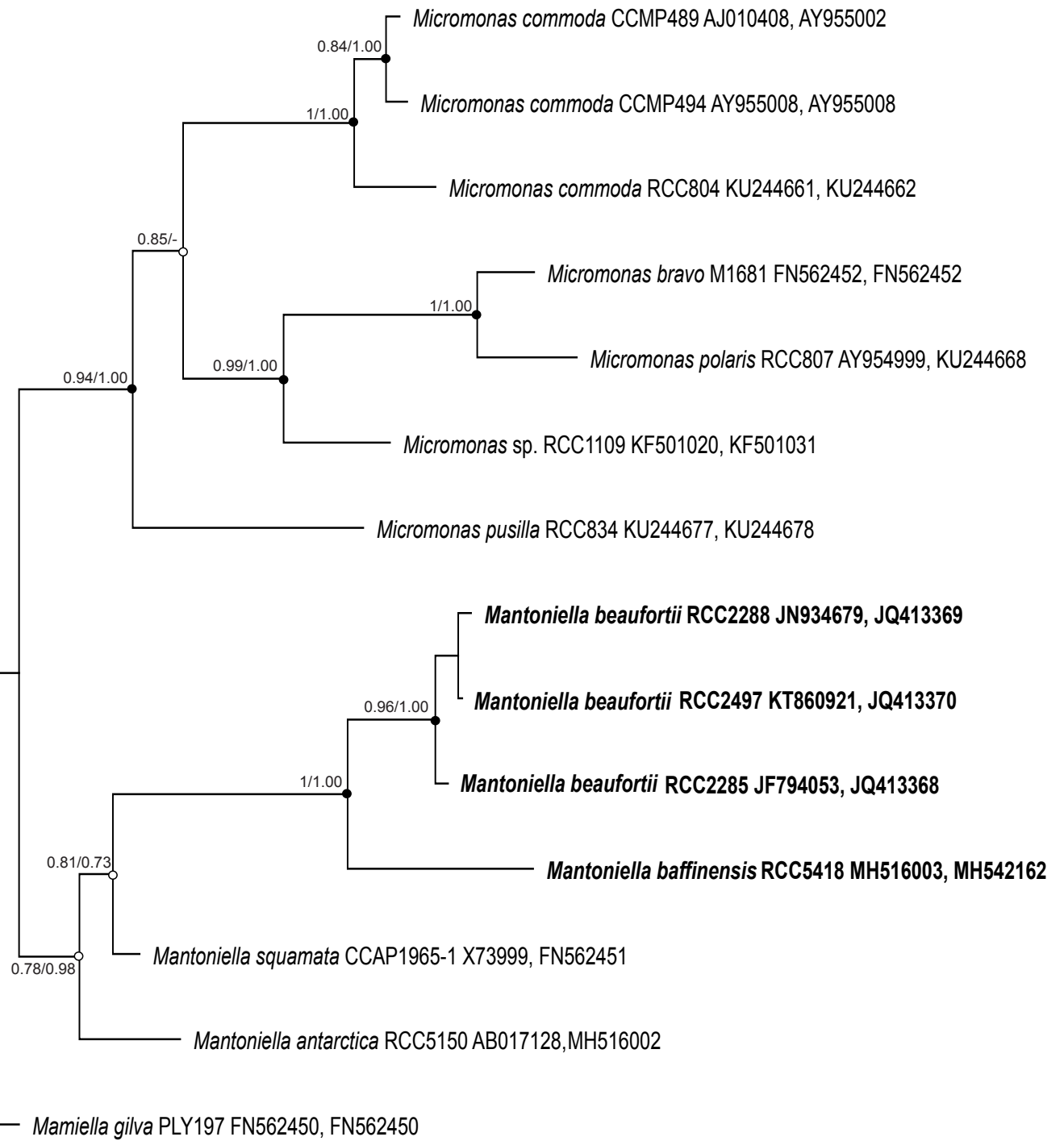
709 Supplementary Material 1: Video microscopy of RCC2288 swimming behavior
710 (<https://youtu.be/CGKNxzfGUvQ>).

711

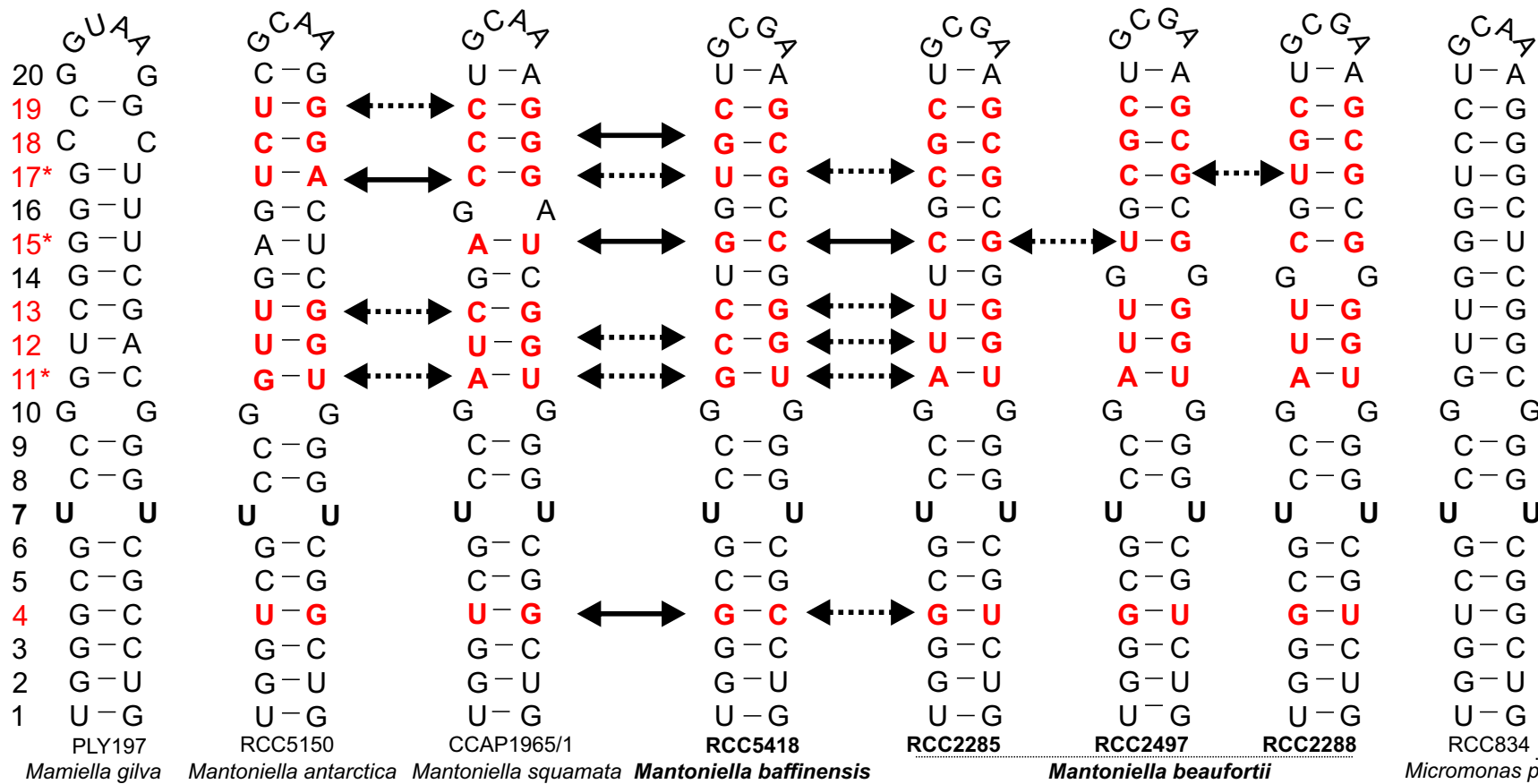
712 Supplementary Material 2: Video microscopy of RCC2497 swimming behavior
713 (<https://youtu.be/rRNuk5Lx7Aw>).

714

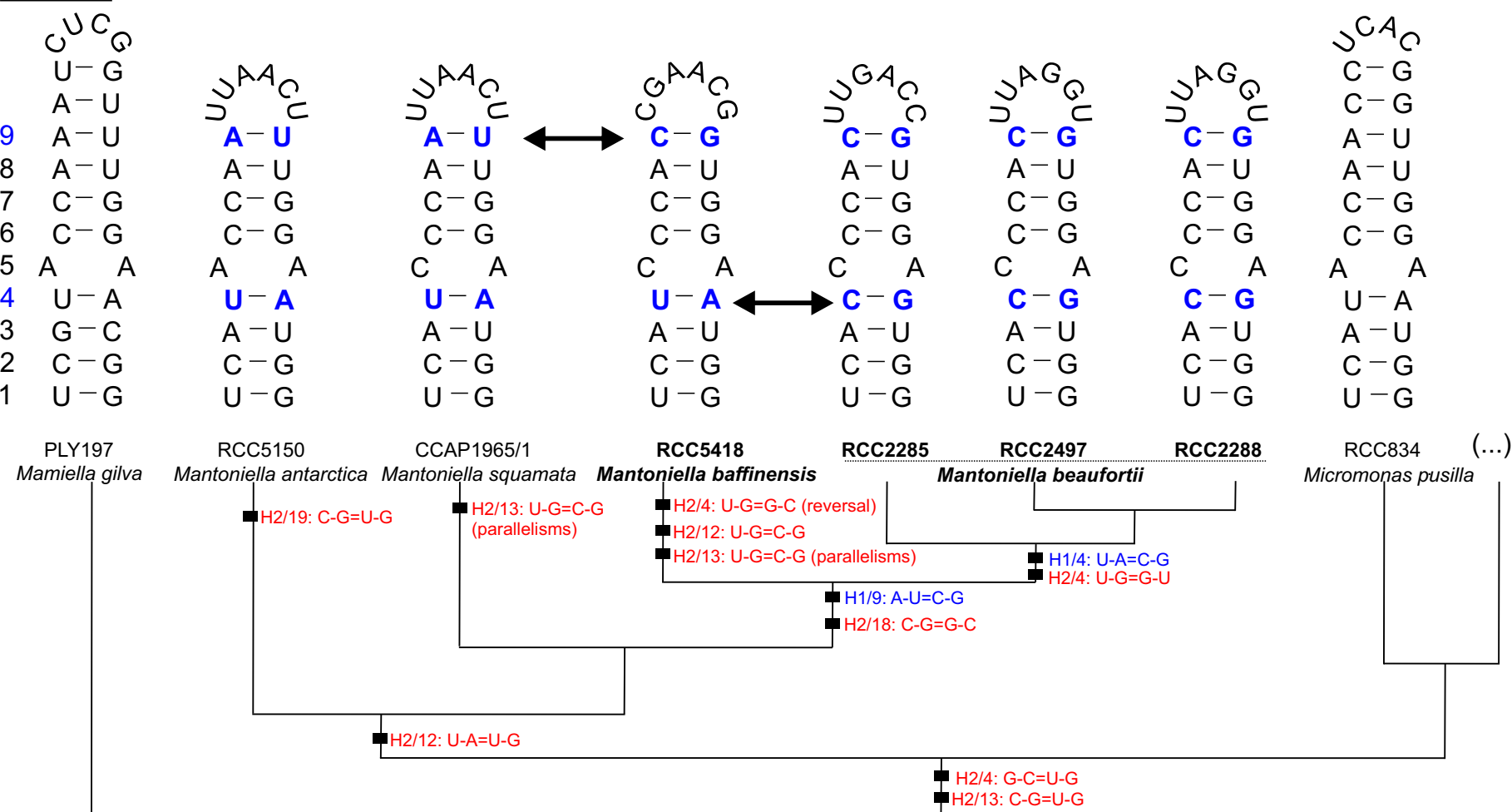
715 Supplementary Material 3: Video microscopy of RCC5418 swimming behavior
716 (<https://youtu.be/xoxCEl1cv4Q>).

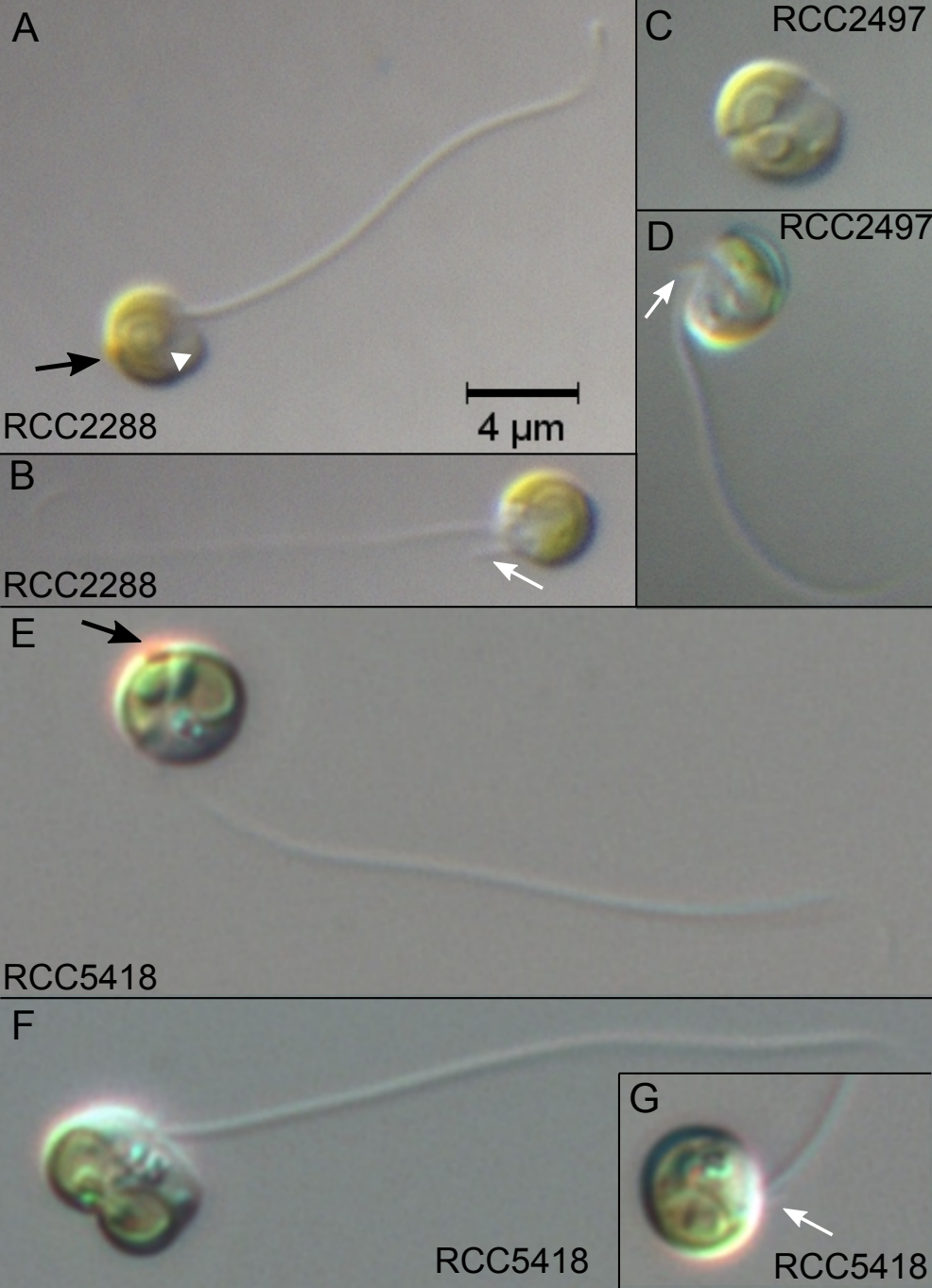


Helix II

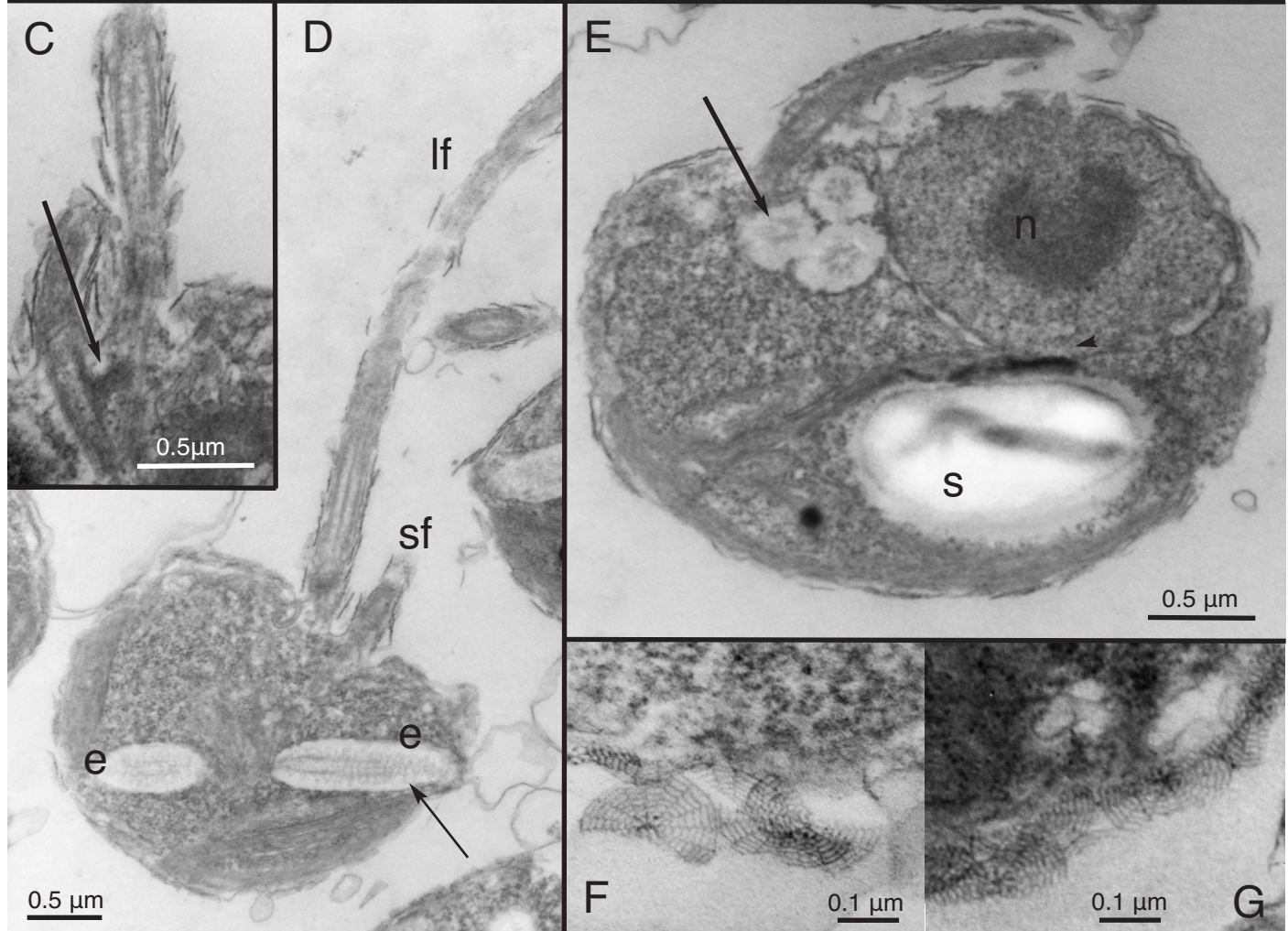
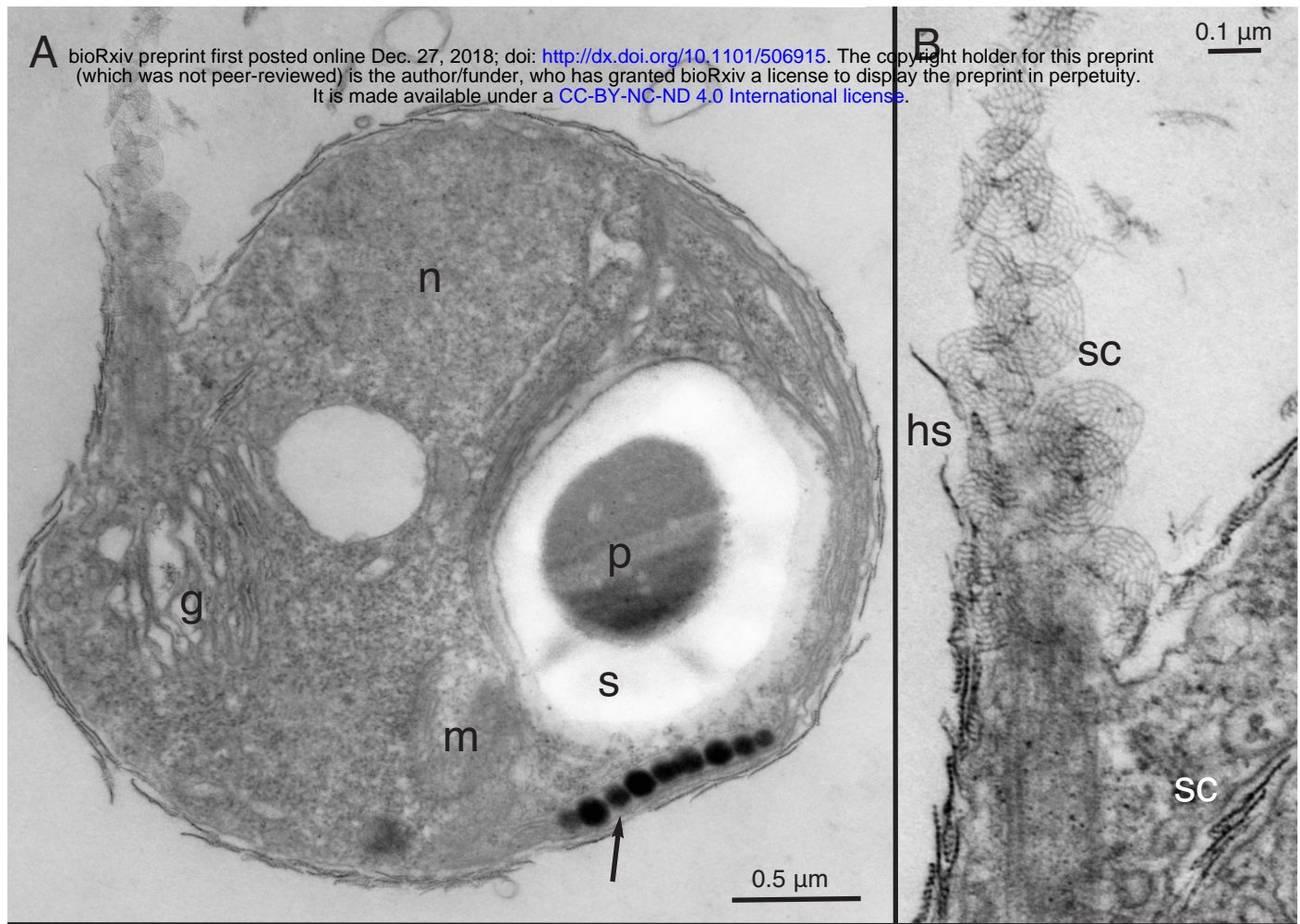


Helix I



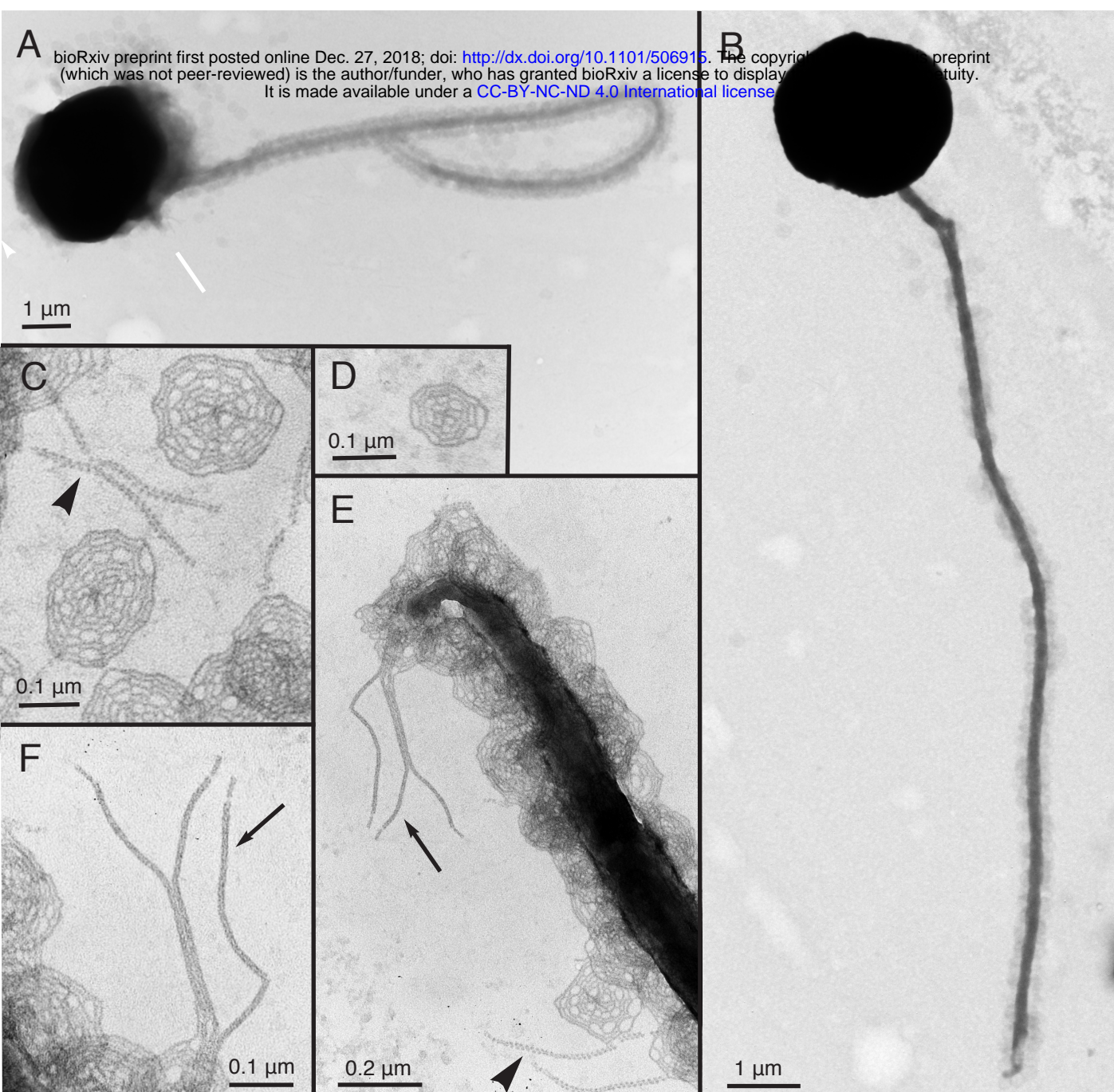


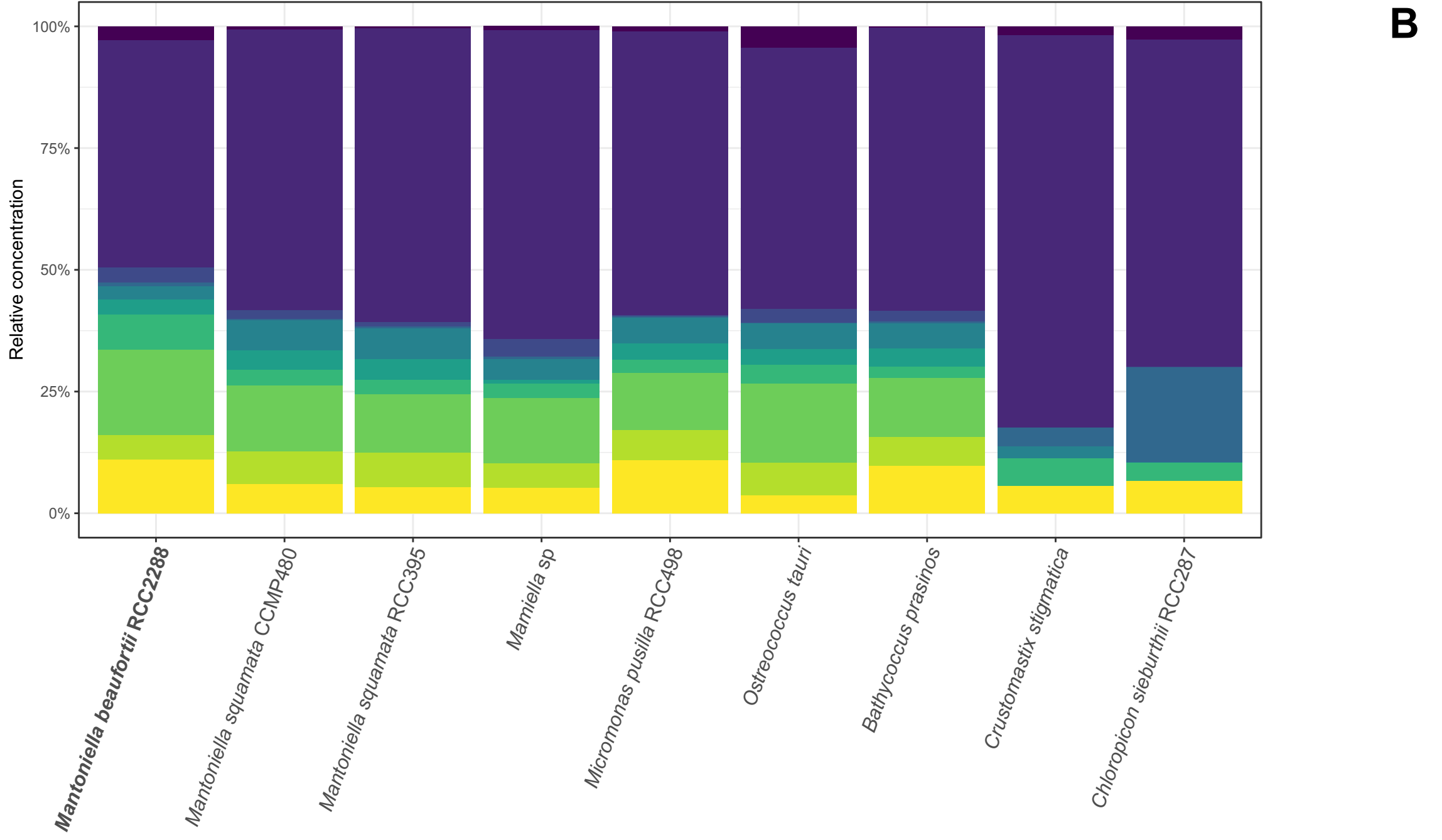
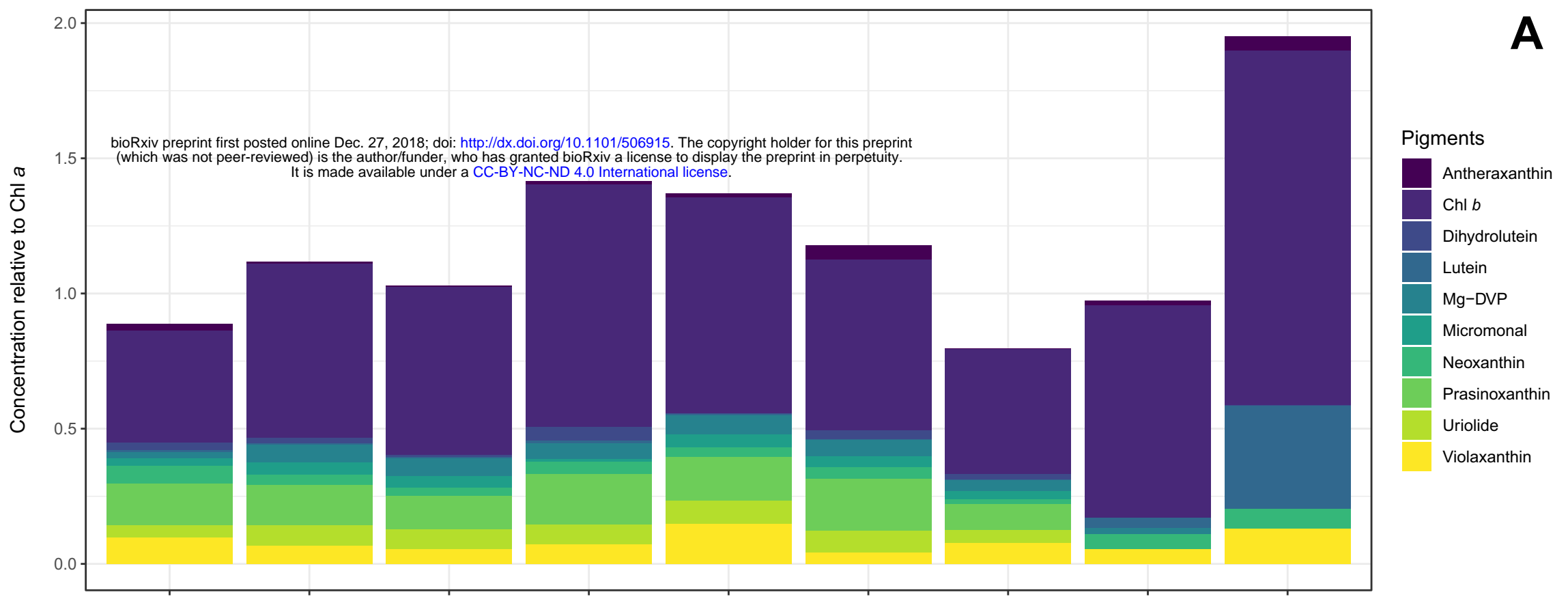
A bioRxiv preprint first posted online Dec. 27, 2018; doi: <http://dx.doi.org/10.1101/506915>. The copyright holder for this preprint (which was not peer-reviewed) is the author/funder, who has granted bioRxiv a license to display the preprint in perpetuity. It is made available under a CC-BY-NC-ND 4.0 International license.

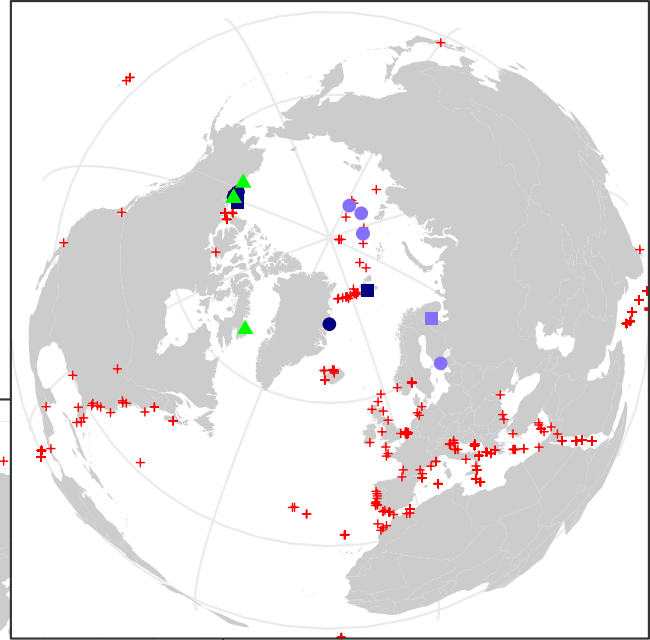
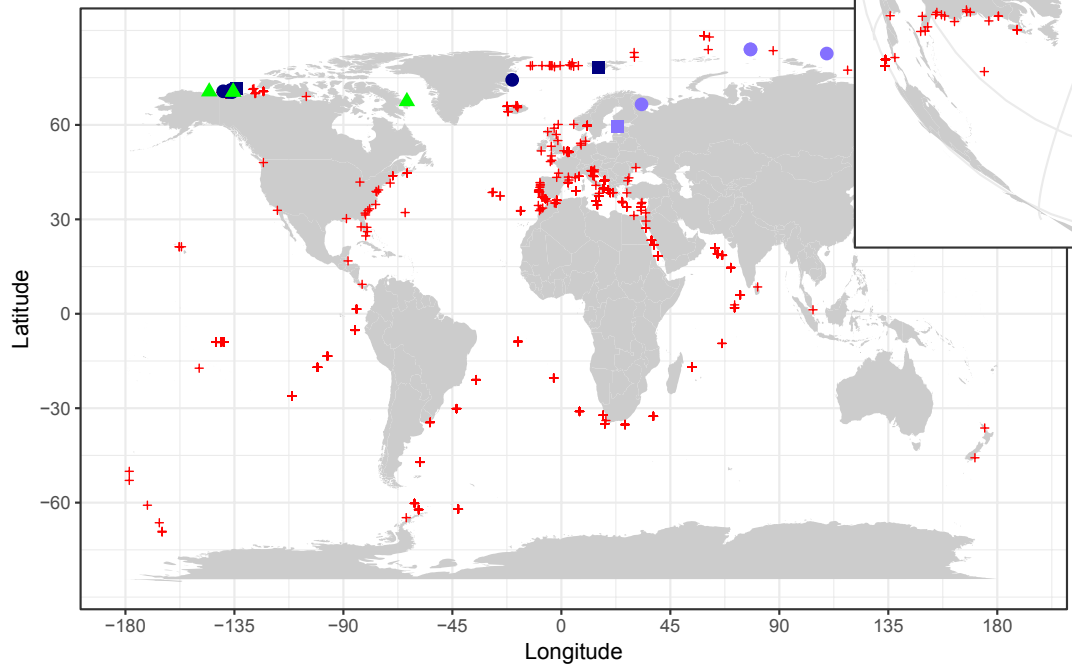


A

bioRxiv preprint first posted online Dec. 27, 2018; doi: <http://dx.doi.org/10.1101/506915>; this version posted December 27, 2018. The copyright holder for this preprint (which was not peer-reviewed) is the author/funder, who has granted bioRxiv a license to display the preprint in perpetuity. It is made available under a CC-BY-NC-ND 4.0 International license.

B**G****H**





- ▲ Culture
- Clone water
- Clone ice
- Meta water
- Meta ice
- + Not found